

Article

Effect of Secondary Phases on Multi-Step Phase Transitions and Magnetocaloric Properties in MnFe-Based Alloys

A-Young Lee ^{1,*}, Min-Ha Lee ², Song-Yi Kim ², JunHee Han ³, Ki-Hoon Kang ¹ and Jong-Woo Kim ¹¹ Department of Functional Ceramics, Korea Institute of Materials Science, Changwon 51508, Republic of Korea² Industrial Materials Processing R&D Department, Korea Institute of Industrial Technology, Yeosu-gu, Incheon 21999, Republic of Korea³ Korea Institute for Rare Metals, Korea Institute of Industrial Technology, Yeosu-gu, Incheon 21999, Republic of Korea

* Correspondence: relaxay@kims.re.kr

Abstract: This study investigated the effect of the secondary phases on multi-step phase transitions and the magnetocaloric properties depending on the Ge content in the MnFeCoPSiGe alloys. Two-step phase transitions were observed by the variations of the Fe₂P-type hexagonal structure (first-order) and secondary phases (second-order). The Curie temperature alters with non-linear behavior consistent with change of the lattice parameters. In addition, the magnetic entropy change decreased with the increase of the Ge content and, subsequently, fractions of the secondary phases. However, the morphological variation of microstructure, distributed as a circular-type shape of the Fe₂P-type hexagonal structure in the Ge-rich matrix, increased the magnetic entropy change. Therefore, the addition of Ge enables the control of the Curie temperature to be applicable for high temperature operating devices. The control of the secondary phases and morphology of the microstructure are crucial to improve the phase transition and magnetic entropy change.



Citation: Lee, A.-Y.; Lee, M.-H.; Kim, S.-Y.; Han, J.; Kang, K.-H.; Kim, J.-W. Effect of Secondary Phases on Multi-Step Phase Transitions and Magnetocaloric Properties in MnFe-Based Alloys. *Metals* **2022**, *12*, 1967. <https://doi.org/10.3390/met12111967>

Academic Editor: Jiro Kitagawa

Received: 12 October 2022

Accepted: 10 November 2022

Published: 17 November 2022

Publisher's Note: MDPI stays neutral with regard to jurisdictional claims in published maps and institutional affiliations.



Copyright: © 2022 by the authors. Licensee MDPI, Basel, Switzerland. This article is an open access article distributed under the terms and conditions of the Creative Commons Attribution (CC BY) license (<https://creativecommons.org/licenses/by/4.0/>).

Keywords: magnetocaloric effect; Fe₂P-type hexagonal structure; multi-step phase transitions

1. Introduction

Magnetocaloric materials have been mostly studied for the rare earth-based alloys that exhibit first-order phase transitions accompanied by large magnetocaloric properties, such as Gd₅Si₂Ge₂ and La(FeSi)₁₃ [1,2]. However, the high cost of raw materials, such as rare-earth elements, has limited the commercial applications of magnetocaloric materials. Among the various magnetocaloric materials, MnFePAs alloy was regarded as suitable for industrial applications due to its significant magnetocaloric properties [3,4]. The use of As was proven to be harmful to humans and environments due to its toxicity; as a result, non-metal elements such as Ge and Si are used to substitute As [5–9].

Generally, MnFePX (X = Ge, Si, and so on) alloys exhibit a Curie temperature (T_c) at near room temperature and have prominent magnetocaloric properties, comparable to that of the Gd₅Si₂Ge₂ alloy. MnFePX (X = Si, Ge) alloys have a Fe₂P-type hexagonal structure in a certain composition range of additional elements. Each atom in the Fe₂P-type structure has preferred sites of 3g (Mn), 3f (Fe), 1b (P), and 2c (Si or Ge). When the additional elements such as Si and Ge are substituted into the Fe₂P-type structure, the lattice parameters can be tuned without crystal structure change. This alteration affects the exchange interactions, Curie temperature, and magnetic entropy change [10].

Additionally, some equilibrium impurity phases can be formed by the compositional variations. For instance, in the case of the La-based alloy, the residual Fe atoms, which would not contribute to the formation of the 1:13 phase, produce α -Fe phase [11]. Similarly, in MnFePX (X = Si, Ge) alloys, impurity phases due to constituent elements can also be generated. The residual constituent elements, which did not contribute to the formation of the Fe₂P-type hexagonal structure, produce the (Mn,Fe)_xSi(Ge)_y secondary phases [12–16].

The secondary phases are located at the grain boundary of Fe₂P phase and increase depending on the residual additional elements [17–19]. A reduction in magnetocaloric properties can be due to the secondary phases. As published, most of the secondary phases show the second-order phase transition [20,21]. Since the second-order phase transition has significantly inferior magnetocaloric properties compared to the first-order phase transition, it is important to reduce the secondary phases to improve the magnetocaloric properties.

Most research has studied materials that exhibit the magnetocaloric effect near room temperature because there are many industrial applications for this, such as air conditioners and commercial refrigerators [22]. The magnetocaloric materials with high T_c above room temperature could be widely considered as candidates for applications in spin-electronics, magnetoresistive devices, and thermomagnetic devices [23,24]. However, there are only a few studies about magnetocaloric materials with a high T_c [25,26].

In this study, the effect of compositional variations of the Si and Ge elements on the formation of secondary phases in MnFeCoPSiGe alloys was investigated. In addition, the multi-step phase transitions and magnetocaloric properties depending on the secondary phases was evaluated.

2. Materials and methods

MnFe_{0.99}Co_{0.01}P_{0.4}Si_{0.6-x}Ge_x ($x = 0, 0.1, 0.3, 0.5, 0.6$) alloys were prepared using Mn₂P (purity of 2N) lumps, and Fe (4N), Co (3N), Si (5N), and Ge (5N) chips. These alloys were synthesized through arc-melting and melt spinning processes in an argon atmosphere. The wheel speed of the melt spinning process was 39.3 m/s. The melt-spun ribbons were annealed for 24 h at 1373 K under high vacuum (10^{-4} Torr), and cooled in the chamber.

The microstructures and stoichiometric compositions were analyzed using a field emission scanning electron microscope (FE-SEM, JEOL, Akishima-shi, Japan) with X-ray energy dispersive spectroscopy (EDS) and electron probe micro-analysis (EPMA, CAMECA, Gennevilliers, France). The phase analysis was carried out using X-ray diffraction (XRD, Bruker, Germany) with Cu- $K\alpha$ radiation at room temperature.

The magnetocaloric properties were measured using vibrating sample magnetometer (VSM) at the physical property measurement system (PPMS, Quantum design Inc. San Diego, CA, USA). The temperature dependence of magnetization (M-T curve) was measured at constant magnetic field ($\Delta H = 0.01$ T) in the temperature range of 150 K to 560 K. The magnetic field dependence of magnetization (M-H curve) was measured in the magnetic field up to 2 T around Curie temperature (T_c) under isothermal conditions. The magnetic entropy change (ΔS_m) and relative cooling power (RCP) were derived from the Maxwell relation under various temperatures around T_c [27].

3. Results and Discussion

Figure 1 shows the microstructures of MnFe_{0.99}Co_{0.01}P_{0.4}Si_{0.6-x}Ge_x ($x = 0, 0.1, 0.3, 0.5, 0.6$) melt-spun ribbon alloys in the wheel side surface. The microstructures were observed on BSE mode in SEM. The bright and dark contrasts correspond to the areas of heavier and lighter elements, respectively. The Si-rich (dark gray), P-rich (light gray), and Ge-rich (bright) regions were confirmed as shown in mapping images. The compositions of each area, marked with the red, pink, and light blue arrows in the BSE images of Figure 1, are summarized in Table 1. The mapping images of Fe and Mn elements confirm the overall distribution, but with higher concentrations in some areas. The Mn elements prefer to be located at P-rich areas, while the Fe elements are concentrated more at Si-rich or Ge-rich areas. According to the previous report [28], the atomic bond between the Fe and Ge atoms at 2c site is stronger than that of the Mn and Ge atoms at 1b site in Fe₂P-type hexagonal structure, hence, it is considered that the Mn-P and Fe-Si/Ge pairs are formed depending on preferred bonding and atomic sites.

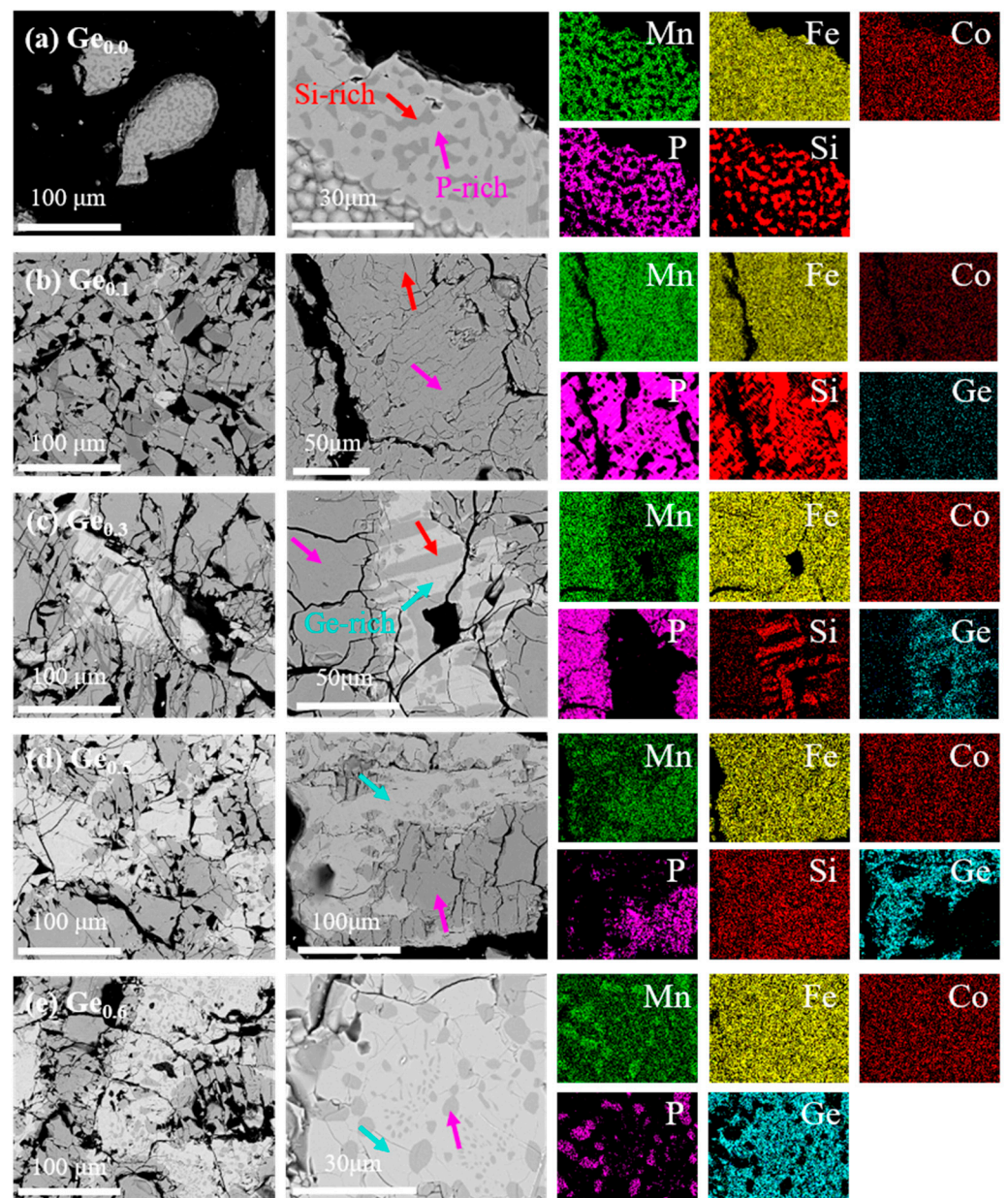


Figure 1. FE-SEM images and corresponding mapping images of the $\text{MnFe}_{0.99}\text{Co}_{0.01}\text{P}_{0.4}\text{Si}_{0.6-x}\text{Ge}_x$ alloys, (a) $\text{Ge}_{0.0}$, (b) $\text{Ge}_{0.1}$, (c) $\text{Ge}_{0.3}$, (d) $\text{Ge}_{0.5}$, (e) $\text{Ge}_{0.6}$. Arrows indicate the rich phase regions. The results are summarized in Table 1.

Table 1. EPMA analysis results of the $\text{MnFe}_{0.99}\text{Co}_{0.01}\text{P}_{0.4}\text{Si}_{0.6-x}\text{Ge}_x$ ($x = 0, 0.1, 0.3, 0.5, 0.6$) alloys as marked region by arrow in Figure 1.

Element (wt.%)	$G_{0.0}$		$G_{0.1}$			$G_{0.3}$		$G_{0.5}$		$G_{0.6}$	
	R ¹	P ²	R	P	B ³	R	P	B	P	B	P
Mn	9.15	23.96	20.58	32.55	21.43	27.19	31.33	21.02	34.43	24.24	31.55
Fe	57.38	52.19	54.36	43.89	36.43	38.48	41.01	40.45	51.68	46.34	40.14
Co	0.78	0.68	0.83	0.86	0.84	0.57	1.15	1.64	1.33	1.57	1.11
P	4.49	15.85	1.16	14.95	0.88	0.49	12.29	1.00	6.82	0.88	15.29
Si	28.20	7.33	20.5	5.16	3.60	13.22	6.36	1.59	1.31	-	-
Ge	-	-	2.57	2.59	36.82	20.05	7.86	34.30	4.43	26.97	11.91

¹ Red arrow, ² Pink arrow, and ³ Light blue arrow.

In addition, the microstructures vary depending on the increase of Ge content. According to the previous research, the secondary phases and precipitates, which are induced by additional elements or heat treatment, are located at the grain boundaries of Fe_2P phases [17–19]. The microstructure of the $\text{Ge}_{0.0}$ alloy is similar to the previous study. The Si-rich areas are distributed on the P-rich matrix. It is considered that the Si-rich phases are located at the grain boundaries of the P-rich phases. As the Ge content increases, the Si-rich and Ge-rich regions are separated and coexist. They exist as independent phases, not grain boundary of the P-rich phases. Moreover, in the $\text{Ge}_{0.6}$ alloy, the P-rich phases separated in the form of a circular-type shape in the Ge-rich matrix.

The $\text{MnFe}_{0.99}\text{Co}_{0.01}\text{P}_{0.4}\text{Si}_{0.6-x}\text{Ge}_x$ ($x = 0, 0.1, 0.3, 0.5, 0.6$) alloys have a Fe_2P -type hexagonal structure (space group $P\bar{6}2m$) and several secondary phases as shown in Figure 2. Although the Ge atoms with bigger atomic radius (125 pm) are substituted for Si (111 pm) atoms, the Fe_2P -type hexagonal structure is maintained. However, the phases of the Fe_2P -type hexagonal structure between the $\text{Ge}_{0.0}$ and the other alloys changed from $\text{FeMnP}_{0.6}\text{Si}_{0.4}$ to $\text{Fe}_{0.94}\text{Mn}_{1.06}\text{P}_{0.8}\text{Ge}_{0.2}$ phase. Moreover, the XRD patterns of the $\text{Fe}_{0.94}\text{Mn}_{1.06}\text{P}_{0.8}\text{Ge}_{0.2}$ phase shifted depending on the Ge content. Most of the diffraction peaks shifted towards a lower angle. It is noted that the (300) and (002) diffraction peaks show different behaviors. The (300) peak moved to low angle and then returned to high angle. On the other hand, the (002) peak shifted from a high angle to a low angle. The movement of the (300) and (002) diffraction peaks signifies the change of lattice parameters [29]. The lattice parameters a and c show non-linear behavior as shown in Figure 3a. The lattice parameter a increases and then decreases, while the lattice parameter c shows the opposite trend. This is consistent with the behaviors of the (300) and (002) diffraction peaks moving from low to high and from high to low angle, respectively. Meanwhile, the unit cell volume expanded gradually with the interplay of the lattice parameters a and c , due to the size effect of the Ge atom.

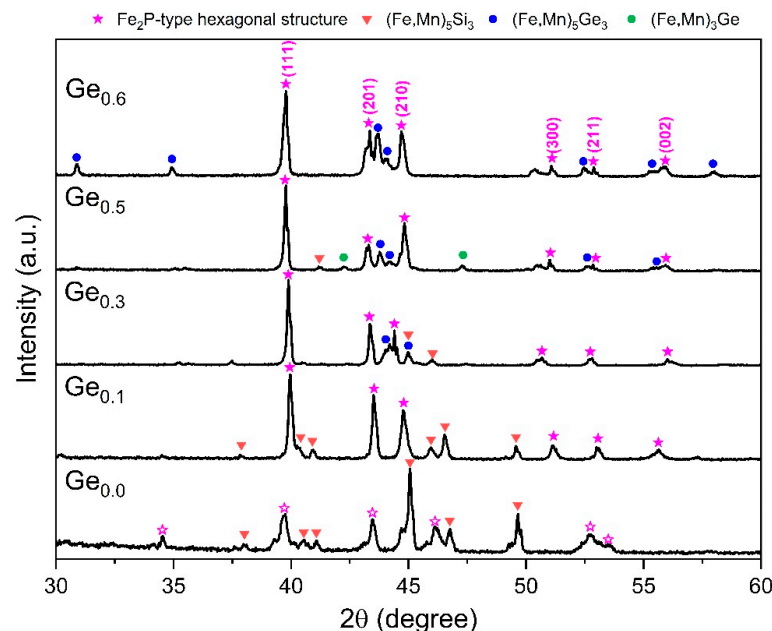


Figure 2. The XRD patterns of the $\text{MnFe}_{0.99}\text{Co}_{0.01}\text{P}_{0.4}\text{Si}_{0.6-x}\text{Ge}_x$ ($x = 0, 0.1, 0.3, 0.5, 0.6$) alloys.

As mentioned above, each area is divided into the P-rich, Si-rich, and Ge-rich regions. It can be matched the Fe_2P -type hexagonal structure, $(\text{Fe,Mn})_5\text{Si}_3$, and $(\text{Fe,Mn})_x\text{Ge}_y$ phases, respectively. The XRD pattern of the $\text{Ge}_{0.0}$ alloy show a different behavior to the other alloys. The diffraction peak intensity for the Fe_2P -type hexagonal structure is dominant in the alloys except for the $\text{Ge}_{0.0}$ alloy. In the case of $\text{Ge}_{0.0}$ alloy, the diffraction peak intensity of the $(\text{Fe,Mn})_5\text{Si}_3$ phase around 45 degrees is higher than that of the Fe_2P -type hexagonal structure. However, the phase fraction of the Fe_2P -type hexagonal structure in the $\text{Ge}_{0.0}$ alloy is higher than that of the $(\text{Fe,Mn})_5\text{Si}_3$ phase as shown in Figure 3b. It is shown that

the diffraction peaks of Fe_2P -type hexagonal structure are broader than that of $(\text{Fe,Mn})_5\text{Si}_3$ phase. The phase fraction of the Fe_2P -type hexagonal structure in the $\text{Ge}_{0.1}$ alloy is the highest of the other alloys. When the small amounts of Ge content are substituted, the fraction of the $(\text{Fe,Mn})_5\text{Si}_3$ phase decreases and subsequently disappears. Meanwhile, the $(\text{Fe,Mn})_3\text{Ge}$ and $(\text{Fe,Mn})_5\text{Ge}_3$ phases appear as the Ge content increases. The secondary phases, which did not contribute to the formation of the Fe_2P -type hexagonal structure, are formed and those fractions increase depending on residual constituent elements [14–16].

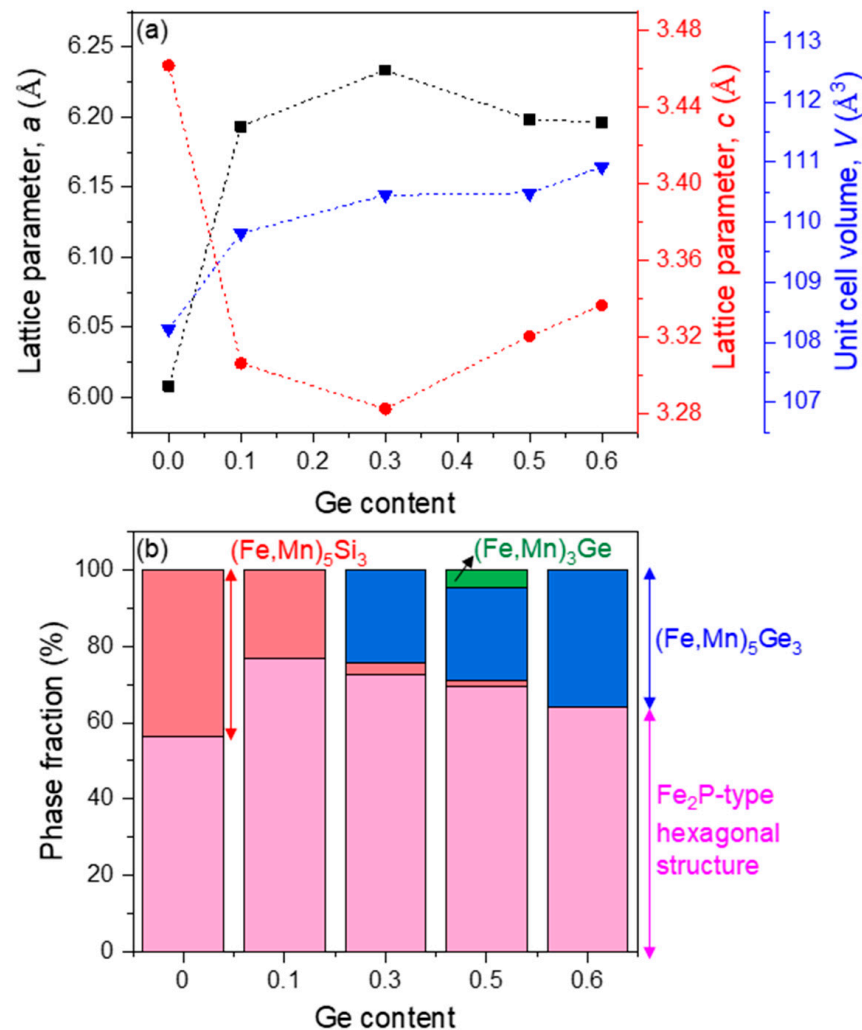


Figure 3. (a) Lattice parameters and unit cell volume, (b) phase fraction of the $\text{MnFe}_{0.99}\text{Co}_{0.01}\text{P}_{0.4}\text{Si}_{0.6-x}\text{Ge}_x$ ($x = 0, 0.1, 0.3, 0.5, 0.6$) alloys.

In addition, the experimental conditions such as the duration, temperature of heat treatment, or composition ratio, significantly affect the formation of secondary phases. Generally, the $(\text{Fe,Mn})_5\text{Si}_3$, $(\text{Fe,Mn})_3\text{Ge}_1$, and $(\text{Fe,Mn})_5\text{Ge}_3$ phases are regarded as secondary phases in Fe_2P -type hexagonal structure; these phases show the second-order phase transition [20,21]. The second-order phase transition has a continuous change in M-T curve compared to the first-order phase transition. The gradual slope change of M-T curve generally results in low ΔS_m . The magnetocaloric properties diminished with the formation of the secondary phases depending on the variation of composition ratio [12–16]. In addition, the presence of particular elements alters the transition and increases the T_c above room temperature [30]. Hence, controlling the amounts of secondary phases plays an important role to improve the magnetocaloric properties.

Figure 4 shows the magnetocaloric properties of $\text{MnFe}_{0.99}\text{Co}_{0.01}\text{P}_{0.4}\text{Si}_{0.6-x}\text{Ge}_x$ ($x = 0, 0.1, 0.3, 0.5, 0.6$) alloys. All the alloys indicate the two-step phase transitions. The formation

of secondary phases as shown in the SEM and XRD results affects the behavior of phase transition. According to Brown et al. [31], there are two occasions in the multi-step phase transitions. One is the transition via an ‘intermediate state’, for instance, from α to β and γ phase. The other is $\alpha_1 \rightarrow \beta_1$ phase and $\alpha_2 \rightarrow \beta_2$ phase at T_1 and T_2 , respectively. In the latter case, the transition between strong parent phase and weak daughter phase is preserved regardless of single or multi-step transitions. Brown et al. reported about the latter transition in $(\text{Mn,Fe})_2(\text{P,Si})$ alloys. They used the magnetic Clausius–Clapeyron equation as given by [31]

$$-\frac{dT_c}{dB} = \frac{\Delta m}{\Delta s} \quad (1)$$

$$\frac{\Delta m_1}{\Delta s_1} = \frac{\Delta m_2}{\Delta s_2} \rightarrow \frac{\Delta m_1}{\Delta m_2} = \frac{\Delta s_1}{\Delta s_2} \quad (2)$$

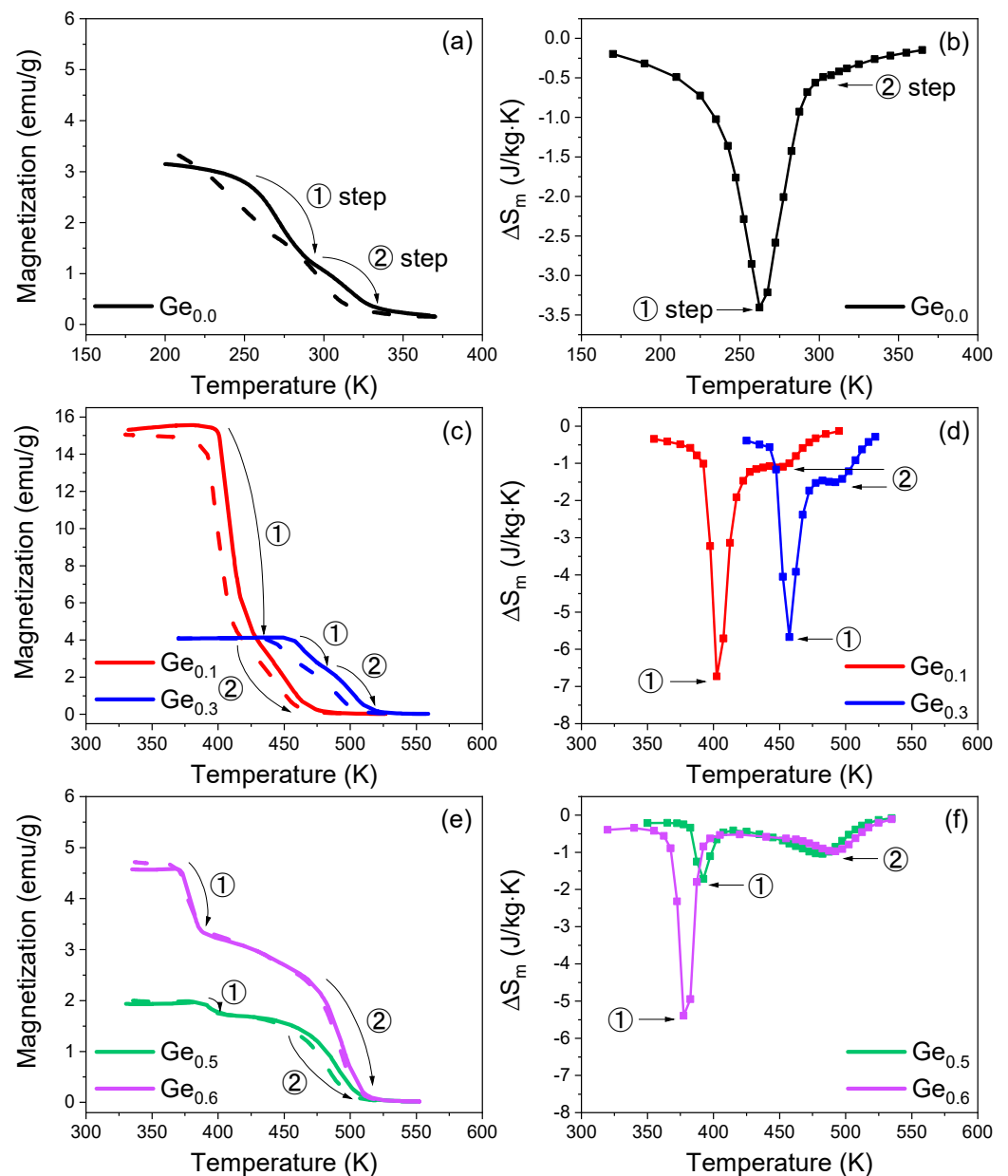


Figure 4. The magnetocaloric properties of the $\text{MnFe}_{0.99}\text{Co}_{0.01}\text{P}_{0.4}\text{Si}_{0.6-x}\text{Ge}_x$ alloys; M-T curve under applied magnetic field (0.01 T) and S-T curve at magnetic field $\Delta H = 2$ T of (a,b) $\text{Ge}_{0.0}$, (c,d) $\text{Ge}_{0.1}$ and $\text{Ge}_{0.3}$, (e,f) $\text{Ge}_{0.5}$ and $\text{Ge}_{0.6}$ alloys.

This transition occurs in the two steps by two almost identical phases, which have small differences in the site ordering or phase compositions. According to the Equations (1) and (2), integral areas of each step transition are almost identical. The $(\text{Mn,Fe})_2(\text{P,Si})$ alloys in the literature showed the transitions of low and high temperature phase with the hexagonal structure. On the other hand, the $\text{MnFe}_{0.99}\text{Co}_{0.01}\text{P}_{0.4}\text{Si}_{0.6-x}\text{Ge}_x$ ($x = 0, 0.1, 0.3, 0.5, 0.6$) alloys in this study show the multi-step phase transitions, different from the latter transition. It can be considered that the two-step phase transitions occurred in the Fe_2P -type hexagonal structure and secondary phases because the integral areas between the transitions show a big difference compared to the characterization from Clausius–Clapeyron equation.

The first step phase transition in all alloys has steeper slope than the second step phase transition, and consequently the ΔS_m of first one is higher. It is thought that the first and second step phase transitions are determined by the Fe_2P -type hexagonal structure and secondary phases, respectively. In addition, the T_c and ΔS_m indicate different behavior with the addition of Ge. In the case of the T_c , that is increased over 370 K with the substitution of Ge atoms compared to the $\text{Ge}_{0.0}$ alloy, and the T_c of the $\text{Ge}_{0.3}$ alloy is the highest. However, the ΔS_m is the largest in the $\text{Ge}_{0.1}$ alloy, and that decreased with the substitution of Ge atoms. These variations are related to the change of lattice parameters and secondary phases [11,32,33]. The drastic change of lattice parameters from the $\text{Ge}_{0.0}$ to the $\text{Ge}_{0.1}$ alloy results in the increase of the T_c to the higher temperature range. Subsequently, the non-linear behavior of lattice parameters affects the identical variation of the T_c . Moreover, the decrease of the ΔS_m is influenced by the increased fraction of secondary phases. The $\text{Ge}_{0.1}$ alloy with the highest ΔS_m has the lowest fraction of secondary phases. As the Ge content increases up to the $\text{Ge}_{0.5}$ alloy, the ΔS_m drastically reduces ($6.73 \text{ J/kg}\cdot\text{K} \rightarrow 1.72 \text{ J/kg}\cdot\text{K}$) due to the increased fraction of secondary phases. Even though the $\text{Ge}_{0.6}$ alloy has the higher fraction of the secondary phase, the ΔS_m increases ($1.72 \text{ J/kg}\cdot\text{K} \rightarrow 5.40 \text{ J/kg}\cdot\text{K}$). According to the previous report [18], heat treatment conditions affect the microstructure and the magnetocaloric properties in the case of Mn-based alloy. Therefore, the $\text{Ge}_{0.6}$ alloy in this study shows the different microstructure with a higher fraction of the secondary phases. This is considered to be a result of the distribution of the phase with Fe_2P -type hexagonal structure forming the circular-type phases in the Ge-rich matrix.

In the second step phase transition by secondary phases, the $(\text{Fe,Mn})_x\text{Ge}_y$ phases induce the transition around 482–492 K in the $\text{Ge}_{0.3}$, $\text{Ge}_{0.5}$, and $\text{Ge}_{0.6}$ alloys, meanwhile, the $(\text{Fe,Mn})_5\text{Si}_3$ phase induces the transition around 447 K in the $\text{Ge}_{0.1}$ alloy. This result is opposed by the magnetocaloric properties in the $\text{Ge}_{0.0}$ alloy. As mentioned above, it is due to the substitution of Ge. Previously, Zhang et al. reported the effect of Si/Ge ratio in Fe_2MnSiGe compounds on the magnetocaloric properties [30]. When the Ge content increases, the T_c increases. According to Candini et al., the T_c of $(\text{Fe,Mn})_5\text{Si}_3$ phase indicates around 250–260 K [34]. In this case, as the Ge element is added, the T_c increased in the phase with the Fe_2P -type hexagonal structure as well as the $(\text{Fe,Mn})_5\text{Si}_3$ phase. In the case of the $\text{Ge}_{0.0}$ alloy, the two steps in M-T curve observed by the phase with the Fe_2P -type hexagonal structure and $(\text{Fe,Mn})_5\text{Si}_3$ phases, but the region of T_c is similar and consequently only one peak is shown in the S-T curve. It is thought that the ΔS_m of the $(\text{Fe,Mn})_5\text{Si}_3$ phase around 320 K is too small, so the behavior of the S-T curve is different from the other alloys. The magnetocaloric properties depending on the Ge content are summarized in Table 2.

Table 2. The magnetocaloric properties of the $\text{MnFe}_{0.99}\text{Co}_{0.01}\text{P}_{0.4}\text{Si}_{0.6-x}\text{Ge}_x$ alloys.

Alloys	Property	T_c (K)	$ \Delta S_m $ (J/kg·K)	RCP (J/kg)
$\text{Ge}_{0.0}$		262	3.41	114.11
$\text{Ge}_{0.1}$		402/447	6.73/1.11	96.35/47.22
$\text{Ge}_{0.3}$		457/492	5.67/1.50	88.30/53.07
$\text{Ge}_{0.5}$		392/482	1.72/1.04	25.44/68.38
$\text{Ge}_{0.6}$		377/492	5.40/0.97	69.92/88.68

4. Conclusions

This study evaluated the effect of the secondary phases on multi-step phase transitions and the magnetocaloric properties of the $\text{MnFe}_{0.99}\text{Co}_{0.01}\text{P}_{0.4}\text{Si}_{0.6-x}\text{Ge}_x$ ($x = 0, 0.1, 0.3, 0.5, 0.6$) alloys. When the Ge content was small, the $(\text{Fe,Mn})_5\text{Si}_3$ phase existed in the Fe_2P -type hexagonal structure. As the Ge content increased, the secondary phases changed from $(\text{Fe,Mn})_5\text{Si}_3$ to $(\text{Fe,Mn})_5\text{Ge}_3$ and $(\text{Fe,Mn})_3\text{Ge}$ phases.

The coexistence of the phase with Fe_2P -type hexagonal structure and the secondary phases affected the magnetocaloric properties as well as the phase transition behavior. Two-step phase transitions were observed in all alloys. The phase transitions of the first and second step are thought to occur due to the Fe_2P -type hexagonal structure and the secondary phases, respectively.

The magnetic entropy change was the highest in the $\text{MnFe}_{0.99}\text{Co}_{0.01}\text{P}_{0.4}\text{Si}_{0.5}\text{Ge}_{0.1}$ alloy, which has a lower fraction of the secondary phase. As the Ge content, and consequently, the fractions of secondary phases increased, the magnetic entropy change decreased. On the other hand, a sharp increase in the magnetic entropy change is observed in the $\text{MnFe}_{0.99}\text{Co}_{0.01}\text{P}_{0.4}\text{Ge}_{0.6}$ alloy. This is because the Ge-rich matrix has a different microstructure distributed as a circular-type phase of the Fe_2P -type hexagonal structure. In addition, the Curie temperature over 370 K was exhibited as Ge was added. The behavior of the Curie temperature was consistent with the non-linear change of the lattice parameters.

Therefore, the $\text{MnFe}_{0.99}\text{Co}_{0.01}\text{P}_{0.4}\text{Si}_{0.6-x}\text{Ge}_x$ ($x = 0, 0.1, 0.3, 0.5, 0.6$) alloys, which indicate the high Curie temperature, can be applied to industrial applications operating at high temperature. Moreover, the control of the formation of the secondary phase and morphology of the microstructure are important to improve the magnetocaloric properties. In future research, the effect of these microstructure changes on magnetocaloric properties will be analyzed in detail and verified through additional studies, such as orientation analysis. In order to expand the application fields, it is necessary to control the Curie temperature below 400 K by changing the content of Ge or other constituent elements in small amounts. This work can hopefully provide useful insights for the development of magnetocaloric materials by tuning the secondary phase and phase transition behavior.

Author Contributions: Conceptualization, M.-H.L. and J.H.; Methodology, A.-Y.L.; Validation, M.-H.L.; Formal analysis, A.-Y.L.; Investigation, S.-Y.K.; Data curation, A.-Y.L.; Writing—original draft, A.-Y.L.; Writing—review & editing, M.-H.L., J.H., K.-H.K. and J.-W.K.; Visualization, S.-Y.K.; Project administration, J.-W.K.; Funding acquisition, J.-W.K. All authors have read and agreed to the published version of the manuscript.

Funding: This study was partly supported by the Fundamental Research Program of the Korea Institute of Material Science (PNK8270) and by the Institute of Information & Communications Technology Planning & Evaluation (IITP) grant funded by the Korean government (MSIT) (No.2022-0-00882, Development of eco-friendly active magnetic regenerator and magnetic cooling system for the thermal managements of ICT parts and products to improve energy efficiency and reduce carbon emission).

Institutional Review Board Statement: Not applicable.

Informed Consent Statement: Not applicable.

Data Availability Statement: The data that support the findings of this study are available from the corresponding author upon reasonable request.

Conflicts of Interest: The authors declare that they have no conflict of interest.

References

1. Moya, X.; Kar-Narayan, S.; Mathur, N.D. Caloric materials near ferroic phase transitions. *Nat. Mater.* **2014**, *13*, 439–450. [[CrossRef](#)] [[PubMed](#)]
2. Brück, E. Developments in magnetocaloric refrigeration. *J. Phys. D Appl. Phys.* **2005**, *38*, R381–R391. [[CrossRef](#)]
3. Bruck, E.; Ilyn, M.; Tishin, A.M.; Tegus, O. Magnetocaloric effects in $\text{MnFeP}_{1-x}\text{As}_x$ -based compounds. *J. Magn. Magn. Mater.* **2005**, *290–291*, 8–13. [[CrossRef](#)]

4. Szymczak, R.; Nedelko, N.; Lewinska, S.; Zubov, E.; Sivachenko, A.; Gribanov, I.; Radelytskyi, I.; Dyakonov, K.; Slawska-Waniewska, A.; Valkov, V.; et al. Comparison of magnetocaloric properties of the $Mn_{2-x}Fe_xP_{0.5}As_{0.5}$ ($x = 1.0$ and 0.7) compounds. *Solid State Sci.* **2014**, *36*, 29–34. [[CrossRef](#)]
5. Hua, S.; Miaoa, X.; Liu, J.; Ou, Z.; Cong, M.; Haschuloo, O.; Gong, Y.; Qian, F.; You, Y.; Zhang, Y.; et al. Small hysteresis and giant magnetocaloric effect in Nb-substituted $(Mn,Fe)_2(P,Si)$ alloys. *Intermetallics* **2019**, *114*, 106602. [[CrossRef](#)]
6. Hoglin, V.; Cedervall, J.; Andersson, M.S.; Sarkar, T.; Hudl, M.; Nordblad, P.; Andersson, Y.; Sahlberg, M. Phase diagram, structures and magnetism of the $FeMnP_{1-x}Si_x$ -system. *RSC Adv.* **2015**, *5*, 8278–8284. [[CrossRef](#)]
7. Miao, X.F.; Hu, S.Y.; Xu, F.; Brück, E. Overview of magnetoelastic coupling in $(Mn, Fe)_2(P, Si)$ -type magnetocaloric materials. *Rare Met.* **2018**, *37*, 723–733. [[CrossRef](#)]
8. Liu, D.M.; Zhang, Z.L.; Zhou, S.L.; Huang, Q.Z.; Deng, X.J.; Yue, M.; Liu, C.X.; Zhang, J.X.; Lynn, J.W. A pathway to optimize the properties of magnetocaloric $Mn_{2-x}Fe_xP_{1-y}Ge_y$ for magnetic refrigeration. *J. Alloys Compd.* **2016**, *666*, 108–117. [[CrossRef](#)]
9. Zhang, Z.L.; Liu, D.M.; Xiao, W.Q.; Li, H.; Wang, S.B.; Liang, Y.T.; Zhang, H.G.; Li, S.L.; Fu, J.J.; Yue, M. Influence of the Ge distribution on the first order magnetic transition of the $MnFe(P,Ge)$ magnetocaloric material. *Phys. Chem. Chem. Phys.* **2018**, *20*, 18117–18126. [[CrossRef](#)]
10. Tu, D.; Yan, J.; Xie, Y.; Li, J.; Feng, S.; Xia, M.; Li, J.; Leung, A.P. Accelerated design for magnetocaloric performance in Mn-Fe-P-Si compounds using machine learning. *J. Mater. Sci. Technol.* **2022**, *96*, 241–247. [[CrossRef](#)]
11. Yan, Y.; Liu, C.; Lu, W.; Sun, Y.; Zhu, W.; Nie, X.; Sang, X.; Zhao, W.; Zhang, Q. Effect of Gd doping on the microstructure and magnetocaloric properties of $LaFe_{11.5}Si_{1.5}$ alloy. *J. Alloys Compd.* **2022**, *910*, 164858. [[CrossRef](#)]
12. Li, C.F.; Zheng, Z.G.; Wang, W.H.; Liu, J.Y.; Lei, L.; Zeng, D.C. Effect of M/NM ratios on structural and magnetic properties of $(Mn,Fe)_2(P,Si)$ compounds. *Phys. B Condens. Matter* **2020**, *594*, 412309. [[CrossRef](#)]
13. TBrown, D.; Galvan, D.; van Buskirk, J.; Mott, A.; Shamberger, P.J. Effect of carbide formation on phase equilibria and compositional modulation of transformation properties in $(Mn,Fe)_2(P,Si)$ alloys. *J. Alloys Compd.* **2020**, *830*, 154532. [[CrossRef](#)]
14. Yan, A.; Müller, K.-H.; Schultz, L.; Gutfleisch, O. Magnetic entropy change in melt-spun $MnFePGe$. *J. Appl. Phys.* **2006**, *99*, 08K903. [[CrossRef](#)]
15. Ou, Z.Q.; Wang, G.F.; Lin, S.; Tegus, O.; Brück, E.; Buschow, K.H.J. Magnetic properties and magnetocaloric effects in $Mn_{1.2}Fe_{0.8}P_{1-x}Ge_x$ compounds. *J. Phys. Condens. Matter* **2006**, *18*, 11577–11584. [[CrossRef](#)]
16. Chen, X.; Repaka, D.V.M.; Ramanujan, R.V. Structural investigation of the crossover in the magnetic transition of Mn-Fe-P-Ge magnetocaloric powders. *J. Alloys Compd.* **2016**, *658*, 104e109. [[CrossRef](#)]
17. Wang, W.H.; Zheng, Z.G.; Huang, B.; Lai, J.W.; Zhou, Q.; Lei, L.; Zeng, D.C. Magnetocaloric effect, corrosion and mechanical properties of $Mn_{1.05}Fe_{0.9}P_{0.5}Si_{0.5}Cu_x$ alloys. *Intermetallics* **2019**, *113*, 106539. [[CrossRef](#)]
18. Zheng, Z.G.; Zhu, Z.R.; Yu, H.Y.; Zeng, D.C.; Li, Y.H.; He, A.; Mozharivskiy, Y. Large magnetic entropy change and magnetic phase transitions in rapidly quenched bulk Mn-Fe-P-Si alloys. *J. Alloys Compd.* **2017**, *725*, 1069–1076. [[CrossRef](#)]
19. Wang, W.H.; Zheng, Z.G.; Li, C.F.; Hong, Y.; Lei, L.; Zeng, D.C. Effect of Cu and B Co-doping on magnetocaloric effect, phase transition, and mechanical properties of $Mn_{1.05}Fe_{0.9}P_{0.5-x}Si_{0.5}Cu_{0.10}B_x$ alloys. *J. Mag. Mag. Mater.* **2021**, *517*, 167380. [[CrossRef](#)]
20. Kim, E.J.; Kang, K.H.; Yoon, C.S. $Mn_xFe_{5-x}Si_3$ for active magnetic regenerative refrigeration at room temperature. *J. Mag. Mag. Mater.* **2021**, *530*, 167952. [[CrossRef](#)]
21. Aryal, A.; Dubenko, I.; Zamora, J.; Llamazares, J.L.S.; Sanchez-Valdes, C.F.; Mazumdar, D.; Talapatra, S.; Stadler, S.; Ali, N. Synthesis, structural, and magnetic properties of Heusler-type $Mn_{2-x}Fe_{1+x}Ge$ ($0.0 \leq x \leq 1.0$) alloys. *J. Mag. Mag. Mater.* **2021**, *538*, 168307. [[CrossRef](#)]
22. Phan, M.H.; Yu, S.C. Review of the magnetocaloric effect in manganite materials. *J. Magn. Magn. Mater.* **2007**, *308*, 325–340. [[CrossRef](#)]
23. Zhu, X.; Dai, Y.; Luo, C. Electronic and magnetic properties of $Co_2Fe(Ga_{1-x}Si_x)$ and $Co_2Fe(Al_{1-y}Si_y)$ Heusler alloys with high Curie temperature. *J. Magn. Magn. Mater.* **2016**, *398*, 7–12. [[CrossRef](#)]
24. Trapanese, M.; Viola, A.; Franzitta, V. Design and experimental test of a thermomagnetic motor. *AASRI Procedia* **2012**, *2*, 199–204. [[CrossRef](#)]
25. Lee, A.Y.; Kim, S.Y.; Oh, H.R.; Kim, H.A.; Kim, Y.D.; Lee, M.H. Effect of synthesis methods on magnetocaloric properties of Co-based Heusler-type alloys. *Mater. Sci. Eng. B* **2018**, *231*, 98–104. [[CrossRef](#)]
26. Wurmehl, S.; Fecher, G.H.; Kandpal, H.C.; Ksenofontov, V.; Felser, C.; Lin, H. Investigation of Co_2FeSi : The Heusler compound with highest Curie temperature and magnetic moment. *Appl. Phys. Lett.* **2006**, *88*, 032503. [[CrossRef](#)]
27. Gschneidner, K.A., Jr.; Pecharsky, V.K. Magnetocaloric materials. *Annu. Rev. Mater. Sci.* **2000**, *30*, 387–429. [[CrossRef](#)]
28. Liu, X.B.; Liu, J.P.; Zhang, Q. Altounian, Fe magnetic moment formation and exchange interaction in Fe_2P : A first-principles study. *Phys. Lett. A* **2013**, *377*, 731–735. [[CrossRef](#)]
29. Wurentuya, B.; Yibole, H.; Guillou, F.; Ou, Z.; Zhang, Z.; Tegus, O. First-order magnetic transition, magnetocaloric effect and moment formation in $MnFe(P,Ge)$ magnetocaloric materials revisited by x-ray magnetic circular dichroism. *Phys. B Condens. Matter* **2018**, *544*, 66–72. [[CrossRef](#)]
30. Zhang, L.; Brück, E.; Tegus, O.; Buschow, K.H.J.; de Boer, F.R. The crystallographic phases and magnetic properties of $Fe_2MnSi_{1-x}Ge_x$. *Phys. B Condens. Matter* **2003**, *328*, 295–301. [[CrossRef](#)]
31. Brown, T.D.; Chen, J.; Braham, E.J.; Stadler, S.; Shamberger, P.J. Dynamic re-equilibration controlled multi-step transformations in $(Mn, Fe)_2(P, Si)$ alloys. *J. Phys. D Appl. Phys.* **2020**, *53*, 205303. [[CrossRef](#)]

32. DThanh, T.C.; Brück, E.; Tegos, O.; Klaasse, J.C.P.; Buschow, K.H.J. Influence of Si and Ge on the magnetic phase transition and magnetocaloric properties of MnFe(P, Si, Ge). *J. Mag. Mater.* **2007**, *310*, e1012–e1014.
33. Song, L.; Wang, G.F.; Ou, Z.Q.; Haschaolu, O.; Tegos, O.; Brück, E.; Buschow, K.H.J. Magnetic properties and magnetocaloric effect of MnFeP_{0.5}Ge_{0.5-x}Si_x compounds. *J. Alloys Compd.* **2009**, *474*, 388–390. [[CrossRef](#)]
34. Candini, A.; Moze, O.; Kockelmann, W.; Cadogan, J.M.; Brück, E.; Tegos, O. Revised magnetic phase diagram for Fe_xMn_{5-x}Si₃ intermetallics. *J. Appl. Phys.* **2004**, *95*, 6819. [[CrossRef](#)]